

Effect of Equal Channel Angular Pressing Processing Routes on Corrosion Resistance and Hardness of Heat Treated A356 Alloy

(Kesan Pemprosesan Laluan Penekanan Sudut Saluran Sama ke atas Rintangan Kakisan dan Kekuatan Haba Dirawat Aloji A356)

MOHAMED A. GEBRIL*, M. ZAIDI. OMAR, NK. OTHMAN & I.F. MOHAMED

ABSTRACT

Equal channel angular pressing (ECAP) via routes A and Bc was used to process heat treated A356 alloy. The samples produced a range of microstructures in order to investigate the effect of straining on its corrosion behavior in 3.5 wt. % NaCl solution and hardness. The ECAP was conducted at room temperature in a mold with channel angle of 120°. The results show that brittle coarse silicon particles were effectively fragmented into smaller size in the Al-rich matrix after the processing. The hardness and corrosion resistance test showed improvement after T5 and T6 heat treatment, preferably to T6 due to wholly changed in silicon particles morphology than T5. The hardness increased with ECAP processing from 60.66 Hv to 1133.47, 124.91 Hv after three passes route Bc and four passes route A, respectively. The evaluation of corrosion resistance of the alloy showed improvement from 0.0424 to 0.00173, 0.00149 mmy⁻¹ after three passes route Bc and four passes route A, respectively. In this research, both strength and corrosion resistance are improved by ECAP processing of A356 alloy using both routes.

Keywords: A356; corrosion rate; ECAP; grain size; heat treatment; microgalvanic cell

ABSTRAK

Dalam kajian ini, kaedah penekanan sudut saluran sama melalui laluan A dan Bc telah digunakan untuk memproses aloji A356 yang dirawat dengan rawatan haba. Sampel dengan pelbagai jenis mikrostruktur telah disediakan untuk mengkaji kesan terikan terhadap kekerasan dan sifat kakisan aloji A356 dalam larutan NaCl 3.5%. Kaedah ECAP dijalankan pada suhu bilik dengan menggunakan acuan yang mempunyai sudut saluran 120°. Keputusan kajian menunjukkan bahawa selepas pemprosesan, partikel silikon kasar dan rapuh bersepai menjadi partikel bersaiz kecil dalam matriks kaya Al. Ujian kekerasan dan ujian ketahanan kakisan menunjukkan bahawa sifat mekanik aloji A356 bertambah baik selepas rawatan haba T5 dan T6, terutamanya T6, disebabkan perubahan morfologi partikel silikon yang begitu ketara. Kekerasan aloji A356 masing-masing meningkat daripada 60.66 Hv kepada 1133.47 Hv dan 124.91 Hv selepas pemprosesan ECAP melalui laluan Bc tiga kali dan laluan A empat kali. Keputusan penilaian menunjukkan bahawa ketahanan kakisan aloji masing-masing meningkat daripada 0.0424 kepada 0.00173 dan 0.00149 mmy⁻¹ selepas pemprosesan ECAP melalui laluan Bc tiga kali dan laluan A empat kali. Oleh itu, dapat disimpulkan bahawa kekuatan dan ketahanan kakisan aloji A356 meningkat dengan menggunakan kaedah pemprosesan ECAP melalui kedua-dua laluan.

Kata kunci: A356; ECAP; kadar kakisan; rawatan haba; saiz butiran; sel mikrogalvanik

INTRODUCTION

A356 aluminum (Al) alloy consists of Al, silicon (Si) and magnesium (Mg). It has good properties, excellent casting characteristic, good fluidity and corrosion resistance in the atmospheric environment. The alloy has been widely applied in the machinery, aircraft and defense industries and particularly in the automotive industry to replace steel components. Si particles shape and distribution have a major effect on mechanical and electrochemical properties of Al-Si alloy.

Pitting is the most common corrosion form of Al and its alloys, particularly in solutions containing Cl⁻ ions. It is well known that oxide film of Al alloys makes it have a good resistance corrosion in the atmospheric environment. Refining of Si particles improve the stability of oxide film

and corrosion resistance of the alloy due to the reduced area ratio of noble eutectic Si particles (cathode) to less-noble eutectic aluminum phase (anode) around Si particles. Moreover, the corrosion current density between local galvanic couples decreases due to the reduction of area ratio of cathode to area ratio of anode (Ac/Aa ratio). Silicon particles with small sizes will make the re-passive process much easy (Fadavi & Tahamtan 2010). The refining of Al-Si-Mg alloy microstructure lead to improvement of mechanical and electrochemical properties due to the refining of the essentially component of eutectic phase from flake shape to fine Si particles morphology (Galvin et al. 2017).

Applied heat treatment lead to modify the Si particles and improve the strength of aluminum alloys through

precipitation-hardening processes that take place as a consequence of changes in the solubility of alloying elements in the matrix with temperature (Mohamed & Samuel 2012).

Ultra-fine materials meet some unique mechanical, chemical and physical properties and high performances due to their small grain sizes. Severe plastic deformation (SPD) is a process used for achievement of ultrafine-grained (UFG) materials. Equal channel angular pressing (ECAP) is considered the most applicable severe plastic deformation (SPD) technique (Kumar et al. 2012; Valiev & Langdon 2006a, 2006b). During ECAP process, the intense plastic strain can be achieved by simple shear, press the sample through a die containing two channels, equal in cross section, intersecting at an angle of Φ with a corner curvature angle (Kawasaki et al. 2011; Xu & Langdon 2003).

The most effective ECAP routes applied to feed materials are route Bc and route A. Some researchers have concluded that route Bc is the most effective route for producing UFG material (Mohamed et al. 2014), whilst others have suggested that route A is more effective (Song et al. 2011). Some researchers reported that grain refinement can improve corrosion resistance of different alloys (Afshari & Dehghanian 2009; Argade et al. 2013; Balyanov et al. 2004; Zheng et al. 2012). Gu et al. (2011) suggested that the grain refinement improved the mechanical property of alloys without increasing the corrosion resistance. Moreover, some researchers found that the grain refinement with ECAP decreased the corrosion resistance of Al–Mg (Son et al. 2007) and pure Mg alloys (Song et al. 2010). On the other hand, a relationship similar to Hall-Petch for grain size depending on the corrosion rate has been proposed (Argade et al. 2012). Therefore, the present work was performed to study the effect of refining microstructure through heat treatment followed by ECAP processing on hardness and corrosion resistance of A356 alloy. The ECAP processing was accomplished through routes Bc and A, as well as the heat treatment accomplished through T5 and T6.

MATERIALS AND METHODS

A commercial A356 alloy (Si- 6.7 wt. % Mg- 0.149 wt. % Fe- 0.126 wt. % Cu- 0.01 wt. % Mn- 0.002 wt. % Zn- 0.006 wt. % Cr- 0.001 wt. % Ti- 0.178 wt. %) were casted in ingot having initial dimensions of 30 mm \times 140 mm thickness and length. The sample was prepared for both T5 and T6 heat treatment, T5 heat treatment was accomplished at 160°C for 5 h while T6 solution heat treatment accomplished at 535°C for 8 h followed by water quench and further aged at 180°C for 3 h (Gebriel et al. 2018). Both as-cast and heat-treated samples were processed by ECAP at room temperature using routes A (where the sample is not rotated between each pass) and route Bc (90° rotation of samples around the linear axis between each pass). All samples were pressed through a circular cross section die channels having an inner angle, F of 120° and outer curvature, Y

of 20°. The microstructure features of the SPD-processed A356 were characterized by optical microscope, FESEM and energy-dispersive X-ray spectroscopy (EDX). All samples were extracted from the circular rods perpendicular to the pressing direction plane and ground through successive grades of Si carbide abrasive papers from P180 to P2000 grit size. The sample was further polished to a mirror like quality using diamond suspension down to 1 μ m. Keller's reagent (1% HF, 1.5% HCl, 2.5% HNO₃, H₂O) was used to show the constituents of the alloys. The scanning electron microscopy (SEM) images were recorded and elemental mapping was performed using EDX with a Zeiss (Merlin/Merlin Compact/Supra 55VP) microscope operated at an accelerated voltage of 15.00 kV.

Quantitative metallography analysis was carried out to measure the grain size according to ASTM E 112. The silicon particle size was measured using Smart Tiffv2 software considering at least 200 particles in each condition. The Vickers hardness tester (micro Vickers hardness tester Zwick Germany; ZHV μ) was used to measure the hardness of the average of three samples per case. The microhardness test was according to ASTM E 384. These samples were also prepared for microstructure analysis using silicon carbide (SiC) papers with grit of 180 to 2000 and followed by polishing process using 1 μ m and 3 μ m of diamond paste (Al₂O₃), the average of three samples was calculated. The corrosion test was carried out at room temperature using a Gramry 3.2 potentiostat which was attached to a three-electrode that formed an electrochemical cell setup in a 3.5 wt. % NaCl solution was prepared as an electrolyte solution and used as a simulated environment for sea water typically exposed to different structures (Arrabal et al. 2013; Mingo et al. 2016). The measurements were carried out in triplicate for each experimental condition in separate experiments. The sample was mounted using Lecoset 7007 epoxy that was cured in air for 24 h before the test. The mounted test material having exposed surface area of 1 cm² to electrolyte was attached to the working electrode. A graphite electrode and a silver/silver chloride (Ag/AgCl) electrode (in 0.6 molL⁻¹ 3.5% NaCl solution) were used as a counter and reference electrodes, respectively. ASTM Standard G102-89 (2010) was used to provide guidance in electrochemical measurements of corrosion rates. The schematic diagram of the experimental work is shown in Figure 1.

RESULTS AND DISCUSSION

MICROSTRUCTURE OF A356 PRE/POST HEAT TREATMENT

Figure 2(a) shows the as-cast Al-6.70% Si alloy that exhibited a typical hypoeutectic solidification structure, which consisted primary dendritic α -Al phase (white phase) surrounded by eutectic mixture (dark phase). The eutectic Si particles morphology was coarse flake. After T5 treatment, the flake morphology of Si particles transferred to coarse acicular and relatively round shape morphology due to low heat treatment temperature during T5 as seen

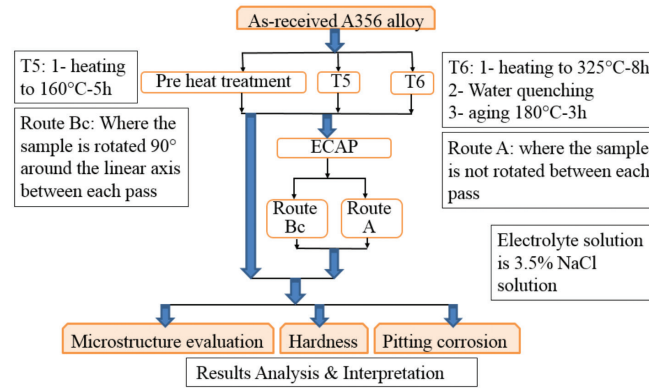


FIGURE 1. Schematic diagram of experimental work

in Figure 2(b). The morphology of the eutectic Si particles obviously changed after the T6 heat treatment, during solution heat treatment flack Si particles break down into smaller fragments and gradually spheroidised (Liu 2009) as in Figure 2(c). A T6 heat treatment improved the alloy more than T5 due to Si particles morphology changed.

MICROSTRUCTURE OF ECAP PROCESSING

Figure 3(a) and 3(b) shows that microstructure of ECAPed as-cast after 2 passes route Bc after T5 and T6, respectively. After 2 passes, the microstructure exhibited irregular morphology after both T5 and T6 heat treatment. The figure shown that some of α -Al solid particles are still sticking together and separation is not completed as shown in Figure 3(a) and 3(b). During the first pass, coarse grains broke into many finer grains with some larger grains around appeared, the grain refinement occurs at the first pass because of higher dislocation rate (Jahadi et al. 2014).

The microstructure of ECAPed as-cast after 2 passes route A after T5 and T6, respectively, is shown in Figure

3(c) and 3(d). At the beginning of route A deformation, shear bands produced rapidly subdivide the coarse grains of the as-cast alloy. After 2 passes route A, it is clear that the microstructure consists of longitudinal grains shape, some grains become more elongated and grain boundaries tend to lie approximately at 45° . The microstructure is relatively inhomogeneous and the eutectic phase is not uniformly distributed in the matrix. The eutectic phase is finer after T6 than T5 in both routes. The average of Si particles and grain size illustrated in Table 1.

Figure 4(a) indicates that an increase of strain through route Bc improves solid morphology such that 3 passes after T6 sample satisfies the minimum requirement of solid globularity. The third pass of as-cast T5 and fourth passes of as-cast T6 route Bc showed cracks up along sample surface. By applying more level of strain through route A, grain width decreases and deformation bands develop within the grains, grain refinement inside the elongated shape, the microstructure became more homogeneous of eutectic mixture surrounded the elongated α -Al phase,

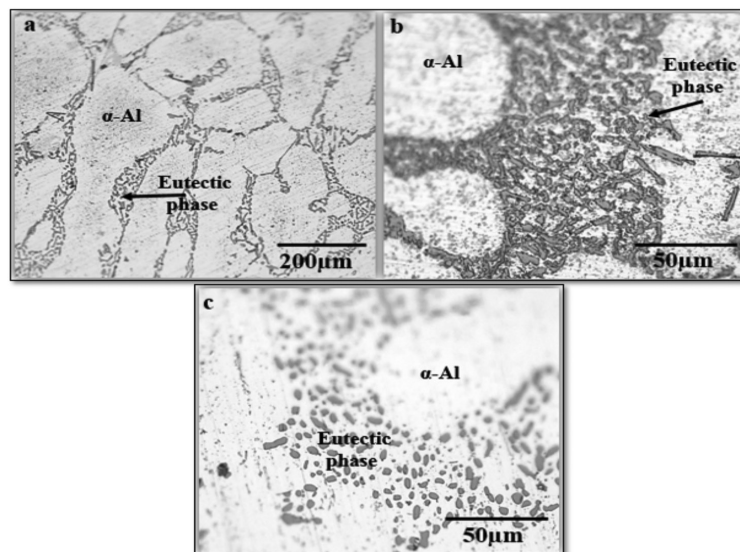


FIGURE 2. Microstructure of A356 alloy (a) as-cast (b) after T5 and (c) after T6

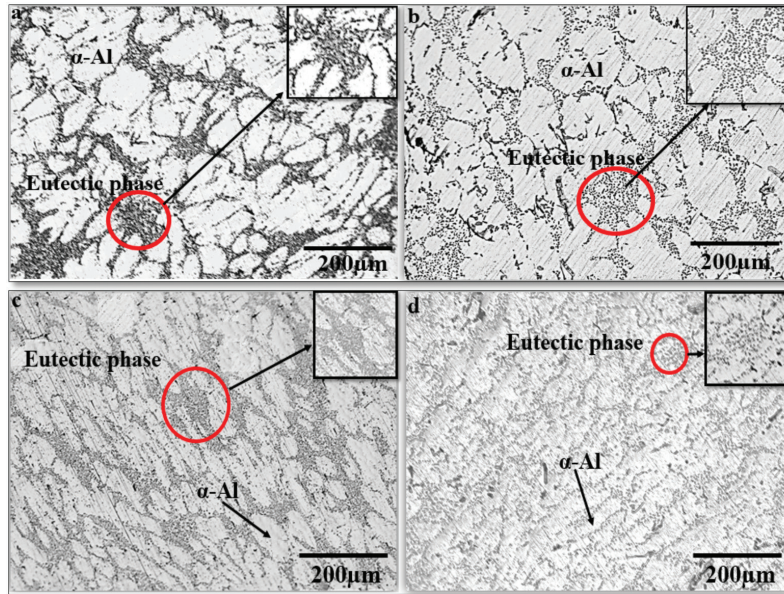


FIGURE 3. Microstructure of ECAPed as-cast sample after 2 passes (a) T5 route Bc (b) T6 route Bc (c) T5 route A and T6 route A (d)

TABLE 1. Average values of grain size and silicon particles size

Pass No. Route	Si particles size (μm)	Grain size (μm)
0 pass	4.22	170.51
0 pass-T5	3.25	163.00
0 passes-T6	2.46	116.00
2 passes Bc	2.54	125.13
2 passes Bc-T5	2.30	78.00
2 passes Bc-T6	1.63	64.61
2 passes A	2.68	105.10
2 passes A-T5	1.987	77.20
2 passes A-T6	1.74	62.85
3 passes Bc-T6	1.33	48.49
4 passes A-T6	0.761	40.40

and the crystallographic contrast increased substantially, as illustrated in figure 4b after 4 ECAP passes post T6 heat treatment. Two important effects can be observed in the microstructure of A356 alloy after ECAP process were: The changes of primary α -Al phase and eutectic mixture phase. As-cast structure was characterized by the typical dendritic shape of α -Al with large and brittle flake morphology of Si particles surrounded the original Al dendrites.

During severe plastic deformation in Bc route, the α -Al phase changed to nearly globular shape after 3 passes post T6. Applied ECAPP via route Bc lead to globularisation microstructure shape of α -Al instead of rheocast process and this was found agreement to Ashouri et al. (2008). While Applied more passes route A lead to longitudinal and fiber shape of α -Al phase.

Table 1 shows the grain size and average of Si particles size of as-cast A356 alloy, after T5, T6 and ECAPed samples. The eutectic Si particles were spheroidised and uniformly distributed at the grain boundaries after T6 and the average

size of as-cast eutectic Si particles decrease from 4.22 to 3.25 and 2.46 μm after T5 and T6, respectively, due to necking and brake down process during T6 heat treatment. ECAP-T6 process broken the coarse Si particles to small equiaxed particles (average size is about 0.761 μm) after 4 passes route A. The grain size of as-cast alloy reduced after ECAP-T6 from 170.51 μm to 40.4 μm after 4 passes due to high dislocation density. Table 1 illustrates the grain size and eutectic Si size are smaller after route Bc than A, because in route Bc the continuous shearing on the three crystallographic planes, the sub-grain boundaries evolve most rapidly into high angle grain boundaries while in route A, the continuous shearing on the two crystallographic planes (Venkatachalam et al. 2010). ECAP process of extruded material led to slightly finer grains than found when processing by heat treatment. Three passes of route Bc can be applied for A356 alloy after T6.

PITTING CORROSION

The influence of the microstructure condition (Heat treatment vs ECAP) on the corrosion resistance was found in Figure 5 and Table 2. Figure 5(a) shows the polarisation curves of as-cast, as-cast after T5 and T6 of A356 aluminium alloy in 3.5% NaCl. The decrease in corrosion rate and increases in the polarisation resistance after T5 and T6 heat treatment can be attributed to eutectic Si morphology changed. After T5 heat treatment the flake morphology of Si particles transferred to acicular shape. While the improvement of corrosion rate after T6 can be attributed to change of Si particles to coarse globular shape substantially. The enhanced corrosion resistance after T6 process is therefore believed to be associated with the following factors: A reduction in the area ratio between the cathodic and anodic phases

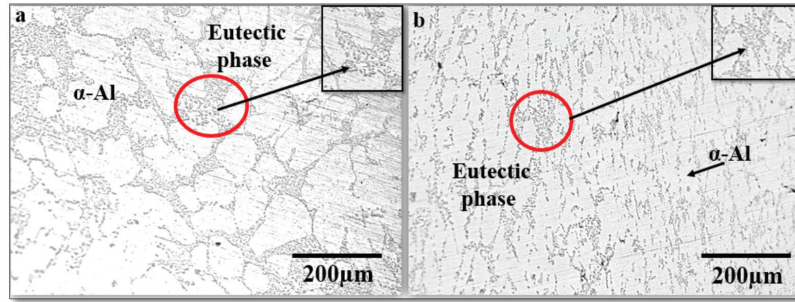


FIGURE 4. Microstructure of ECAPed-T6 as-cast sample (a) after passes 3 Passes route Bc and (b) after 4 passes route A

due to globularisation of Si particles, homogeneity of α -Al dendrites (Ogris et al. 2002), and precipitation of Mg_2Si phase that have anodic action with respect to the aluminium matrix, which may enhance localized corrosion (Yasakau et al. 2007).

Figures 5(b) and 5(c) shows the polarisation curves of ECAPed A356 alloy after two passes routes Bc and A, respectively, and after T5 and T6. The corrosion rate of ECAPed heat treated A356 alloy decreased after two passes in both routes Bc and A comparing with heat treated as-cast alloy. The corrosion resistance of ECAPed A356 alloy was improved due to fragmentation of silicon particles and also the reduction in grain size due to severe plastic deformation during ECAP process that reduced the microgalvanic effect. Figure 5(d) shows the polarization curves of ECAPed-T6, 3 passes route Bc, and ECAPed-T6, 4 passes A. Fragmentation of Si particles and homogeneity of the microstructure will be reduced the galvanic potential difference as a result of the reduced area ratio between noble Si particles and less-noble eutectic phase

(Park et al. 2005). Corrosion rate was improved from 0.0424 mmy^{-1} for as-cast to 0.00173 and 0.00149 mmy^{-1} after T6 heat treatment of ECAPed, 3 passes route Bc and 4 passes route A, respectively. The improvement of corrosion resistance in route Bc can be attributed to the structure refinement. The evaluation of ECAP process microstructure between routes A and Bc showed that path Bc is most effective for microstructure refining (Iwahashi et al. 1998). In the potentiodynamic test, the corrosion rate of A356 alloy decreased with increasing the number of ECAP pass times in both routes Bc and A as shown in Table 2.

Figure 6(a) and 6(b) shows the surface appearance of as-cast and as-cast ECAPed-T6 4 passes route A samples, after ten days of immersion process in 3.5% NaCl solution. The visual investigation of the corroded surface of both samples shows the corrosion occurs in the eutectic phase area while the α -Al phase remains unattacked, the pits formed by localised corrosion attack between the active particles and the noble particles in the eutectic phase

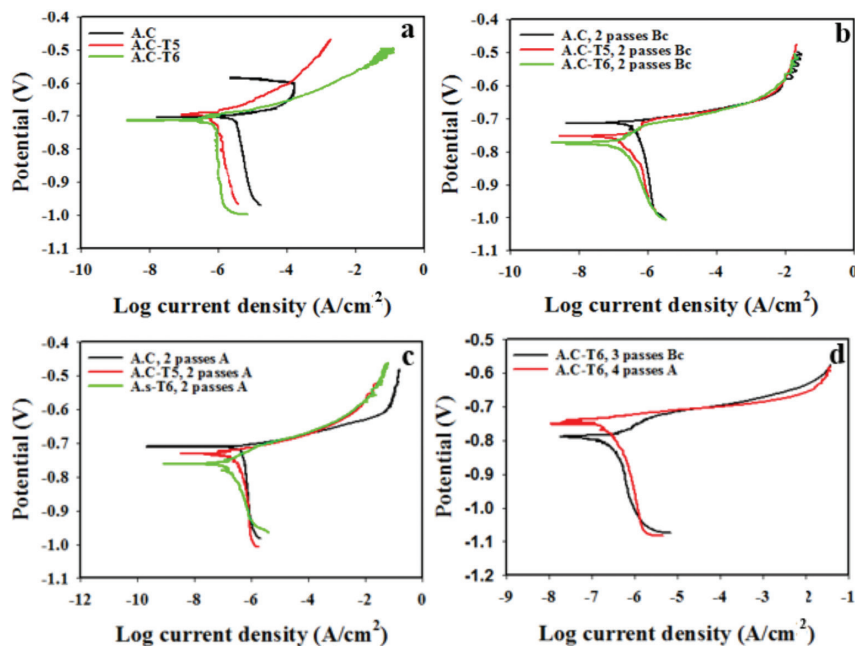


FIGURE 5. Polarization curves of T5 and T6 unECAPed as-cast (a), ECAPed 2 passes route Bc (b), ECAPed 2 passes route A (c) and ECAP 3 passes Bc and 4 passes A (d)

TABLE 2. Average values of polarization resistance (R_p) and corrosion rate (CR) evaluated from Figure 5

Pass No. Route	R_p (Ωcm^2)	CR (mmpy^{-1})
0 pass	5.215×10^3	0.0424
0 pass-T5	1.913×10^4	0.0160
0 passes-T6	2.035×10^4	0.0092
2 passes Bc	7.912×10^4	0.0104
2 passes Bc-T5	9.726×10^4	0.0025
2 passes Bc-T6	1.408×10^5	0.00196
2 passes A	2.713×10^4	0.00671
2 passes A-T5	5.287×10^4	0.00320
2 passes A-T6	9.026×10^4	0.00218
3 passes Bc-T6	1.26×10^5	0.00173
4 passes A-T6	9.147×10^4	0.00149

exhibited a larger size in as-cast alloy in comparison to the pit size for ECAPed surface. It was indicated from the presence of pits surrounded with large rings product that their condition was stable (Son et al. 2007). It was implied from the corrosion products being absent in the rings which surrounded the pits indicated that there are no dissolved aluminium ions in solution within the rings but the corrosion occurred inside the pits due to concentration galvanic cells (Callister & Rethwisch 2012). Figure 6(c) and 6(d) shows the side view of as-cast and as-cast ECAPed-T6 4 passes route A after Potentiodynamic test in 3.5% NaCl solution. The corroded area on the alloy's surface increases because of the presence of the eutectic phase increased area in the as-cast compared to as-cast ECAPed-T6 4 passes sample. In the image, it can be clearly seen as some of primary α -Al grains were separated because of corrosion in eutectic phase, which surrounded these grains. Figure 6(d) shows the side view of corroded surface morphology of as-cast ECAPed after 4 passes in which the surface microstructure appears more fine and

homogenous with fibrous-like shapes as well as shows the difference in the α -Al separated grains' area and depth of corrosion in the eutectic mixture phase between both the as-cast and ECAPed samples.

HARDNESS

Figure 7 demonstrates the effects of T5 and T6 heat treatment as well as ECAP processes following route A and Bc on the hardness of A356 alloy. Improvement of A356 alloy after heat treatment can be attributed to morphology changing of Si particles from coarse flake particles which negatively affect the mechanical properties to acicular Si particles morphology after T5 heat treatment. The spheroidisation of eutectic Si after T6 heat treatment was found to increase the hardness of samples. Essentially, the spheroidisation of Si particles after T6 heat treatment and precipitation of magnesium silicide (Mg_2Si) particles during aging process tend to increase ultimate tensile strength as well as hardness (Möller 2012; Zhu 2017).

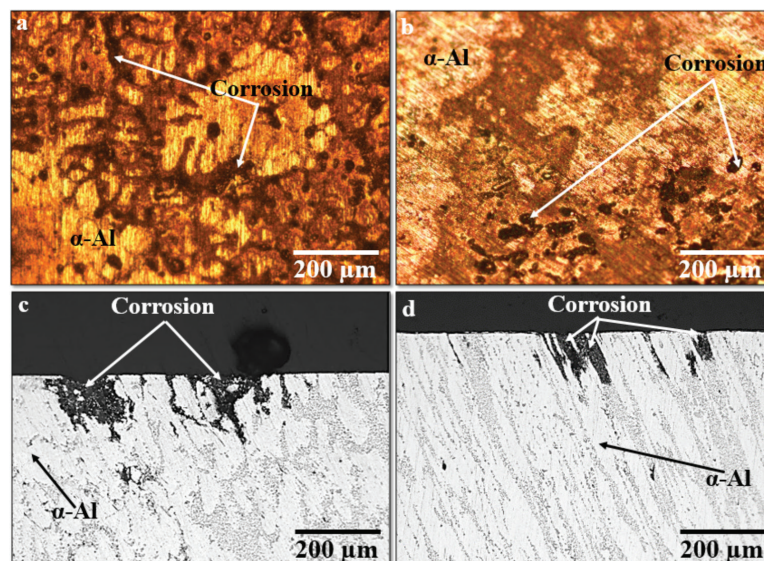


FIGURE 6. Pitting corrosion of A356 alloy after 10 days' immersion in 3.5 wt. % NaCl solution (a) as-cast, (b) ECAPed 4 passes, pitting corrosion after Potentiodynamic test of (a) as-cast and (d) ECAPed 4 passes

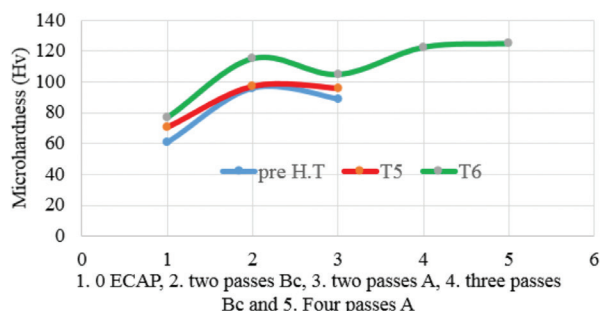


FIGURE 7. Microhardness of ECAPed heat treated ECAPed A356 alloy

As it is clear from this figure, the average of hardness values is increased with increasing the pass number. After the second ECAP passes, the microstructure is still in of inhomogeneous and the appearance of the dendritic form was disappearance, the primary α -Al phase tended to be spheroidising via route Bc while elongated shape via route A and the Si particles became a fragmented result of increase in hardness in all samples. Also, it has been reported that with imposing deformation, brittle and hard eutectic Si particles are broken and with increasing the deformation, their mean free space becomes smaller. Since the strength is inversely related to the mean free space of particles, the hardness values of samples are increased with increasing the pass number (Haghshenas & Sabetghadam 2009; Haghshenas et al. 2009). Three passes of ECAP route Bc and four passes of ECAP route A increased the hardness of both samples due to the fragmentation of eutectic Si particles, the reduction in grain size, and aging process. The homogenous distribution of Si particles and primary α -Al phase of the ECAPed route A plays an integral role in improving the hardness of ECAPed materials.

CONCLUSION

Investigating the electrochemical properties and the hardness of heat treated ECAPed A356 with routes A and Bc and a various number of passes in 3.5 wt. % NaCl solution; the following conclusion was drawn:

Si particles morphology play a major role in electrochemical and mechanical properties improvement in A356 alloy. Using the ECAP process for reducing the grain size and Si particles size can be accomplished using route A as well as route Bc; nevertheless, route A is more suitable for A356 than route Bc. The solution heat treatment T6 suitable more than T5 due to changed morphology of Si particles content and precipitation of Mg_2Si particles after aging process which improves the hardness of A356 alloy. In particular, the ECAP passes and hence the microstructural evolution and Si particles fragmentation with redistribution at grain boundaries plays a dominant role in decreasing the corrosion rate and increased the polarization resistance due reduced the area ratio of cathode to anode (A_c/A_a) in microgalvanic affect. A fine-grained structure with more grain boundary area reduces chloride concentration

per grain boundary area resulting in less current density. Enhanced corrosion resistance after T5 and T6 can be attributed to depletion of Si and Mg from the matrix due to the formation of strengthening precipitates on aging increases the resistance to corrosion. The ECAP process can be used as one of advanced techniques to produce ultrafine grained bulk materials having better corrosion resistance and hardness through enhances the distribution of eutectic mixture throughout the material. Eutectic Si particles become smaller and more homogeneously distributed, therefore better spatial distribution leads to better stabilization of the layer due to decrease the ratio of cathode to anodic area. Thus, the pitting corrosion resistance can be increased with increasing the number of ECAP passes times.

ACKNOWLEDGEMENTS

The authors acknowledge the Ministry of Higher Education, Malaysia for the Fundamental Research Grant Scheme (FRGS/1/2016/TK03/UKM/02/4).

REFERENCES

- Afshari, V. & Dehghanian, C. 2009. Effects of grain size on the electrochemical corrosion behaviour of electrodeposited nanocrystalline Fe coatings in alkaline solution. *Corrosion Science* 51(8): 1844-1849.
- Argade, G.R., Kumar, N. & Mishra, R.S. 2013. Stress corrosion cracking susceptibility of ultrafine grained Al-Mg-Sc alloy. *Materials Science and Engineering A* 565: 80-89.
- Argade, G.R., Panigrahi, S.K. & Mishra, R.S. 2012. Effects of grain size on the corrosion resistance of wrought magnesium alloys containing neodymium. *Corrosion Science* 58: 145-151.
- Arrabal, R., Mingo, B., Pardo, A., Mohedano, M., Matykina, E. & Rodríguez, I. 2013. Pitting corrosion of rheocast A356 aluminium alloy in 3.5 wt. % NaCl solution. *Corrosion Science* 73: 342-355.
- Ashouri, S., Nili-Ahmadabadi, M., Moradi, M. & Iranpour, M. 2008. Semi-solid microstructure evolution during reheating of aluminum A356 alloy deformed severely by ECAP. *Journal of Alloys and Compounds* 466(1-2): 67-72.
- Balyanov, A., Kutnyakova, J., Amirkhanova, N.A., Stolyarov, V.V., Valiev, R.Z., Liao, X.Z. Zhao, Y.H., Jiang, Y.B., Xu, H.F., Lowe, T.C. & Zhu, Y.T. 2004. Corrosion resistance of ultra fine-grained Ti. *Scripta Materialia* 51(3): 225-229.
- Callister, J.W.D. & Rethwisch, D.G. 2012. *Fundamentals of Materials Science and Engineering: An Integrated Approach*. New York: John Wiley & Sons.
- Fadavi, B.A. & Tahamtan, S. 2010. Effect of a novel thixoforming process on the microstructure and fracture behavior of A356 aluminum alloy. *Materials and Design* 31(8): 3769-3776.
- Galvin, E., O'Brien, D., Cummins, C., Mac Donald, B.J. & Lally, C. 2017. A strain-mediated corrosion model for bioabsorbable metallic stents. *Acta Biomaterialia* 55(9): 505-517.
- Gebril, M.A., Omar, M.Z., Mohamed, I.F., Othman, N.K. & Abdelgnei, M.A.H. 2018. Corrosion improvement and microstructure evaluation of SEM-Solid A356 alloy by ECAP process. *Journal of Physics: Conference Series* 1082(1): 012110.

- Gu, X.N., Li, N., Zheng, Y.F., Kang, F., Wang, J.T. & Ruan, L. 2011. *In vitro* study on equal channel angular pressing AZ31 magnesium alloy with and without back pressure. *Materials Science and Engineering B: Solid-State Materials for Advanced Technology* 176(20): 1802-1806.
- Haghshenas, M. & Sabetghadam, H. 2009. The room temperature mechanical properties of a thermo-mechanically processed Thixocast A356 aluminum alloy. *Journal of Alloys and Compounds* 477(1-2): 250-255.
- Haghshenas, M., Zarei-hanzaki, A. & Jahazi, M. 2009. An investigation to the effect of deformation-heat treatment cycle on the eutectic morphology and mechanical properties of a Thixocast A356 alloy. *Materials Characterization* 60(8): 817-823.
- Iwahashi, Y., Furukawa, M., Horita, Z., Nemoto, M. & Langdon, T.G. 1998. Microstructural characteristics of ultrafine grained aluminum produced using equal-channel angular pressing. *Metallurgical and Materials Transactions A* 29(9): 2245-2252.
- Jahadi, R., Sedighi, M. & Jahed, H. 2014. ECAP effect on the micro-structure and mechanical properties of AM30 magnesium alloy. *Materials Science and Engineering A* 593: 178-184.
- Kawasaki, M., Figueiredo, R.B. & Langdon, T.G. 2011. An investigation of hardness homogeneity throughout disks processed by high-pressure torsion. *Acta Materialia* 59(1): 308-316.
- Kumar, S.R., Gudimetla, K., Venkatachalam, P., Ravisankar, B. & Jayasankar, K. 2012. Microstructural and mechanical properties of Al 7075 alloy processed by Equal Channel Angular Pressing. *Materials Science and Engineering A* 533: 50-54.
- Liu, G.Y. 2009. Effect of ageing heat treatment on the hardness and tensile properties of aluminum A356.2 casting alloy. Thesis. Mechanical Engineering. McMaster University (Unpublished).
- Mingo, B., Arrabal, R., Pardo, A., Matykina, E. & Skeldon, P. 2016. 3D study of intermetallics and their effect on the corrosion morphology of rheocast aluminium alloy. *Materials Characterization* 112: 122-128.
- Mohamed, A.M.A. & Samuel, F.H. 2012. A review on the heat treatment of Al-Si-Cu/Mg casting alloys. *Conventional and Novel Applications* doi: 10.5772/2798.
- Mohamed, M.R., Zaafarani, N.N., El Rahman Salleh, Abd, C. & M. Khourshid, A.E.F. 2014. The effect of compression rate on hardness for pure Al, Al-5083, and Al-1050 with equal channel angular pressing. *International Journal of Scientific & Engineering Research* 5(12): 356-360.
- Möller, H., Govender, G. & Stumpf, W. 2012. Factors influencing tensile mechanical properties of Al-7Si-Mg casting alloys A356/7. In *Lights Metals 2012*, edited by Suarez, C.E. Switzerland: Springer. pp. 467-471.
- Ogris, E., Wahlen, A., Lüchinger, H. & Uggowitzner, P.J. 2002. On the silicon spheroidization in Al-Si alloys. *Journal of Light Metals* 2(4): 263-269.
- Park, C., Kim, S., Kwon, Y., Lee, Y. & Lee, J. 2005. Mechanical and corrosion properties of rheocast and low-pressure cast A356-T6 alloy. *Materials Science and Engineering A* 391(1-2): 86-94.
- Son, I.J., Nakano, H., Oue, S., Kobayashi, S., Fukushima, H. & Horita, Z. 2007. Pitting corrosion resistance of anodized aluminum alloy processed by severe plastic deformation. *Materials Transactions* 48(1): 21-28.
- Song, D., Ma, A.B., Jiang, J.H., Lin, P.H. & Zhang, L.Y. 2011. Improvement of pitting corrosion resistance for Al-Cu alloy in sodium chloride solution through equal-channel angular pressing. *Progress in Natural Science: Materials International* 21(4): 307-313.
- Song, D., Ma, A.B., Jiang, J., Lin, P., Yang, D. & Fan, J. 2010. Corrosion behavior of equal-channel-angular-pressed pure magnesium in NaCl aqueous solution. *Corrosion Science* 52(2): 481-490.
- Valiev, R.Z. & Langdon, T.G. 2006a. Development in the use of ECAP processing for grain refinement. *Reviews on Advanced Materials Science* 13(1): 15-26.
- Valiev, R.Z. & Langdon, T.G. 2006b. Principles of equal-channel angular pressing as a processing tool for grain refinement. *Progress in Materials Science* 51(7): 881-981.
- Venkatachalam, P., Ramesh Kumar, S., Ravisankar, B., Thomas Paul, V. & Vijayalakshmi, M. 2010. Effect of processing routes on microstructure and mechanical properties of 2014 Al alloy processed by equal channel angular pressing. *Transactions of Nonferrous Metals Society of China (English Edition)* 20(10): 1822-1828.
- Xu, C. & Langdon, T.G. 2003. Influence of a round corner die on flow homogeneity in ECA pressing. *Scripta Materialia* 48(1): 1-4.
- Yasakau, K.A., Zheludkevich, M.L., Lamaka, S.V. & Ferreira, M.G.S. 2007. Role of intermetallic phases in localized corrosion of AA5083. *Electrochimica Acta* 52(27): 7651-7659.
- Zheng, Z.J., Gao, Y., Gui, Y. & Zhu, M. 2012. Corrosion behaviour of nanocrystalline 304 stainless steel prepared by equal channel angular pressing. *Corrosion Science* 54(1): 60-67.
- Zhu, M. 2017. Effects of T6 heat treatment on the microstructure, tensile properties, and fracture behavior of the modified A356 alloys. *Journal of Materials & Design* 36: 243-249.
- Mohamed A. Gebril*, M. Zaidi. Omar & I.F. Mohamed
Department of Mechanical and Materials Engineering
Faculty of Engineering and Build Environment
Universiti Kebangsaan Malaysia
43600 UKM Bangi, Selangor Darul Ehsan
Malaysia
- Mohamed A. Gebril*
Department of Mechanical Engineering
Faculty of Engineering, Benghazi University, Benghazi
Libya
- NK. Othman
School of Applied Physics
Faculty of Science and Technology
Universiti Kebangsaan Malaysia
43600 UKM Bangi, Selangor Darul Ehsan
Malaysia
- I.F. Mohamed
Fuel Cell Institute
Universiti Kebangsaan Malaysia
43600 UKM Bangi, Selangor Darul Ehsan
Malaysia
- *Corresponding author; email: gebril.ukm@gmail.com

Received: 8 June 2018

Accepted: 25 December 2018